

# Performance of a gliding arc plasmatron pilot reactor with integrated carbon bed and recirculation for upscaled CO<sub>2</sub> conversion

*Robbe Bryssinck*<sup>‡\*1,2,3,4</sup>, *Gregory James Smith*<sup>‡1,2</sup>, *Colin O'Modhrain*<sup>‡1,2</sup>, *Tom Van Assche*<sup>3</sup>,  
*Georgi Trenchev*<sup>‡4</sup>, *Annemie Bogaerts*<sup>‡1,2</sup>

<sup>1</sup>Research group PLASMANT, Department of Chemistry, University of Antwerp, Universiteitsplein 1, 2610 Wilrijk, Belgium

<sup>2</sup>Electrification Institute, University of Antwerp, Olieweg 97, 2020 Antwerp, Belgium

<sup>3</sup>Department of Chemical Engineering, Vrije Universiteit Brussel, Pleinlaan 2, 1050 Brussel, Belgium

<sup>4</sup>D-CRBN, Olieweg 95, 2020 Antwerp, Belgium

‡ These authors share first authorship. † These authors share senior authorship.

\* corresponding author. E-mail: [robbe.bryssinck@uantwerpen.be](mailto:robbe.bryssinck@uantwerpen.be)

## Supplementary Information

## Table of contents

|   |    |
|---|----|
| <b>Section S1. Picture of the D-CRBN pilot reactor setup</b> .....  | 2  |
| <b>Section S2. 3D fluid flow model of the plasma reactor: Geometry, equations and calculated gas velocity profile</b> ..... | 4  |
| <b>Section S3. 2D axis-symmetric model of the plasma reactor</b> .....  | 6  |
| <b>Section S4. Additional information for the 2D post-plasma chamber model</b> .....  | 8  |
| <b>Section S5. Boundary conditions of the 2D post-plasma chamber model</b> .....  | 8  |
| <b>Section S6. Temporal change of particle diameter</b> .....   | 10 |
| <b>References</b> .....   | 10 |

**Section S1. Picture of the D-CRBN pilot reactor setup**

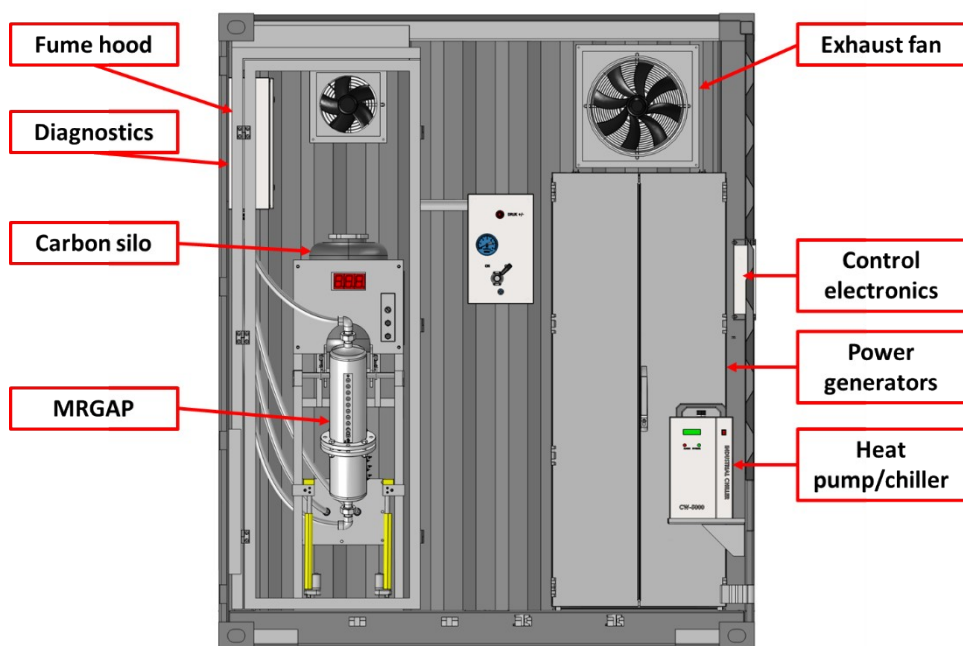


**Figure S1:** Drawing of the D-CRBN pilot container setup.

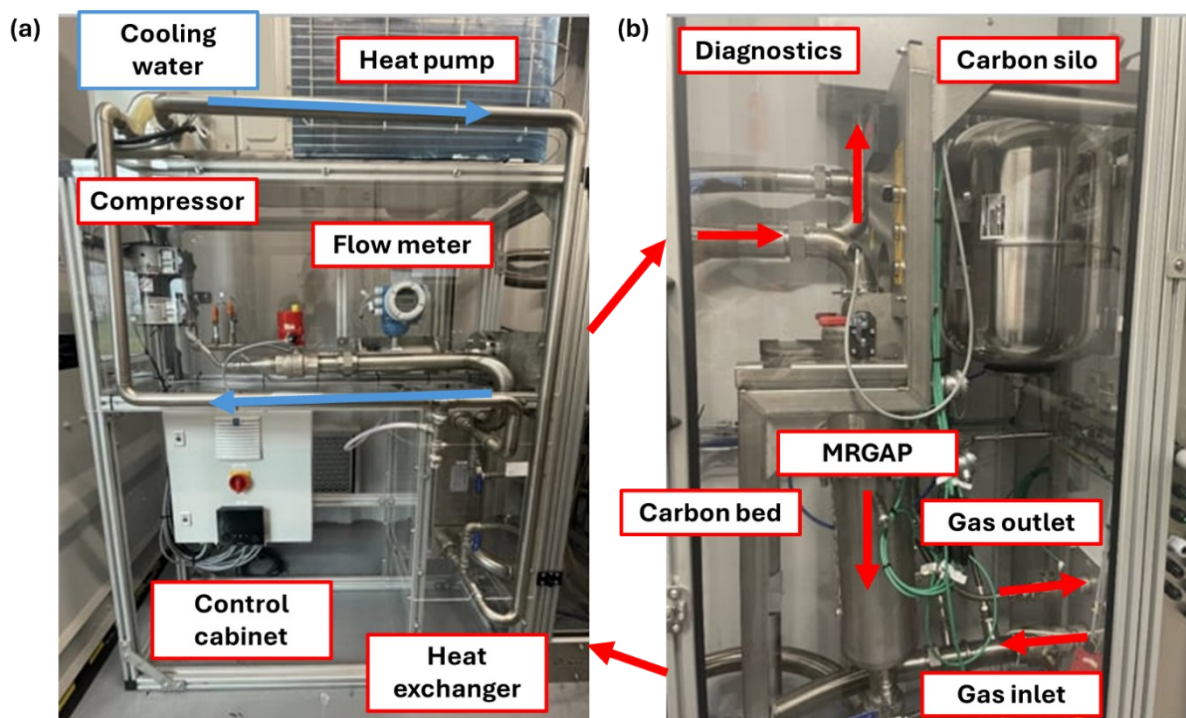


**Figure S2:** Setup of the pilot container, including (a) the heat pump, heat exchanger, recycling system and control cabinet, and (b) the reactor (MRGAP), carbon bed with carbon silo, diagnostics box, and gas connections. The blue arrows in (a) indicate the cooling water circuit, and the red arrows in (b) indicate the gas flow.

Fig. S2 shows the setup inside of the container. The gas flow is shown in red and the blue arrows represent the flow of the cooling water.

### Section S2. 3D fluid flow model of the plasma reactor: Geometry, equations and calculated gas velocity profile

We developed a 3D model of the plasma reactor (focusing on a single gliding arc plasmatron (GAP)), to retrieve the correct flow pattern for the 2D axisymmetric model. The mesh used consists of 341,120 mesh elements. The geometry of the model is depicted in Figure S3.

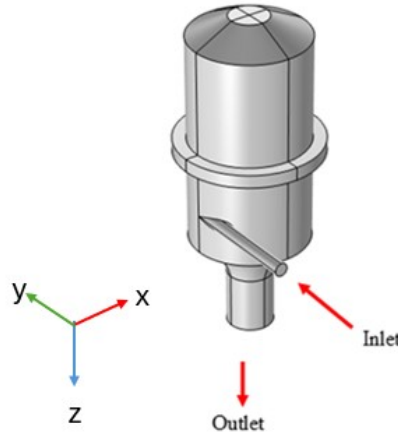


**Figure S3.** 3D geometry of the plasma reactor (single GAP) model.

The 3D fluid flow model is solved by describing the gas flow in the reactor with the Menter's Shear Stress Transport (SST) turbulent flow model with weakly compressible flow. In the model, the following Reynolds-Averaged Navier-Stokes (RANS) equations are solved<sup>1</sup>:

$$\nabla \cdot \rho \mathbf{u} = 0 \quad (S1)$$

$$\rho(\mathbf{u} \cdot \nabla)\mathbf{u} = \nabla \cdot \left[ -p\mathbf{I} + (\mu + \mu_T)\left(\nabla\mathbf{u} + (\nabla\mathbf{u})^T - \frac{2}{3}(\mu + \mu_T)(\nabla \cdot \mathbf{u})\mathbf{I} - \frac{2}{3}\rho k\mathbf{I}\right) \right] \quad (S2)$$

Where  $\rho$  ( $\text{kg m}^{-3}$ ) stands for the gas density calculated by the thermodynamic model,  $\mathbf{u}$  ( $\text{m s}^{-1}$ ) is the gas flow velocity vector,  $p$  (Pa) is the gas pressure,  $\mathbf{I}$  is the unity tensor,  $\mu$  ( $\text{kg m}^{-1} \text{s}^{-1}$ ) is the dynamic viscosity,  $\mu_T$  ( $\text{kg m}^{-1} \text{s}^{-1}$ ) is the turbulent dynamic viscosity,  $k$  ( $\text{W m}^{-1} \text{K}^{-1}$ ) is the turbulent kinetic energy, and superscript  $T$  stands for transposition.

The 3D velocity profile in the single GAP reactor results from the reverse-vortex flow profile. Figure S3a shows the z-x projection of the 3D model, where the red line (at  $z = 19$  mm) indicates the location at which the velocity profiles are transferred to the 2D axisymmetric model. Figure S3b shows the cut plane at this position, to obtain the velocity in cylindrical coordinates as a function of the radius. Here, the average velocity value is taken in three cylindrical coordinates ( $r, \varphi, z$ ) to construct the 2D axisymmetric inlet velocity profile.

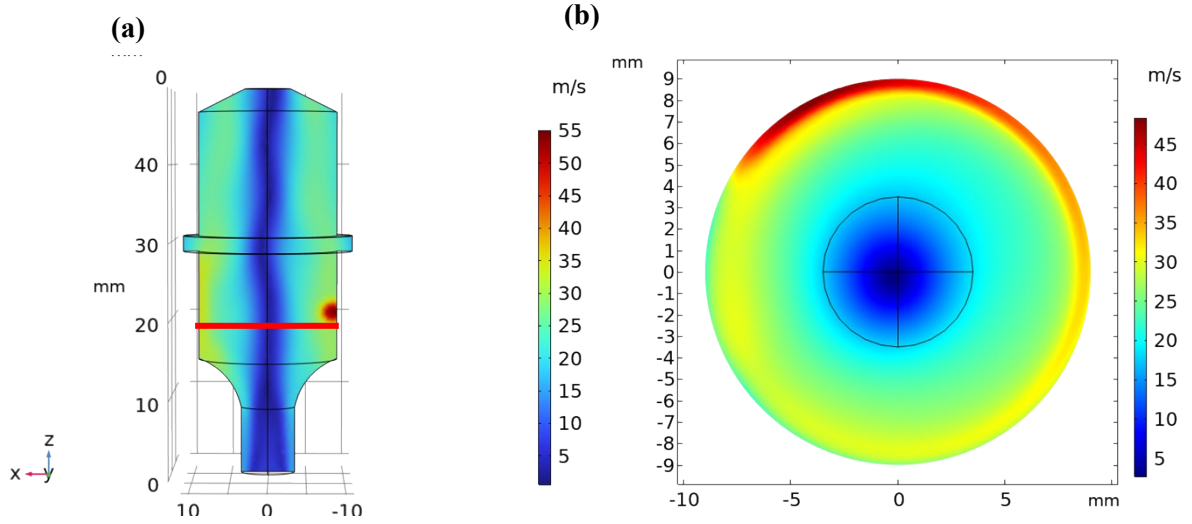


**Figure S4.** Velocity profile in (a) the entire GAP reactor (z-x projection) and (b) the x-y cut plane, to obtain the 2D axisymmetric inlet velocity for the 2D model.

The Cartesian velocity coordinates are translated to cylindrical coordinates using the following equations<sup>2</sup>:

$$v_r = \frac{dr}{dt} = \frac{d}{dt}(\sqrt{x^2 + y^2}) = \frac{xv_x + yv_y}{\sqrt{x^2 + y^2}}$$

$$v_\varphi = r \frac{d\varphi}{dt} = \sqrt{x^2 + y^2} \frac{d}{dt} \left( \tan^{-1} \left( \frac{y}{x} \right) \right) = \frac{xv_y - yv_x}{\sqrt{x^2 + y^2}}$$

$$v_z = v_z \tag{S5}$$

### Section S3. 2D axis-symmetric model of the plasma reactor

The CFD plasma reactor model is used to provide the correct inlet velocity and temperature profile for our 2D model of the post-plasma chamber with carbon bed (described in the main paper). To make the computational time feasible, we used a 2D axisymmetric geometry. The geometry consists of 198,261 mesh elements and is shown in Figure S5a.

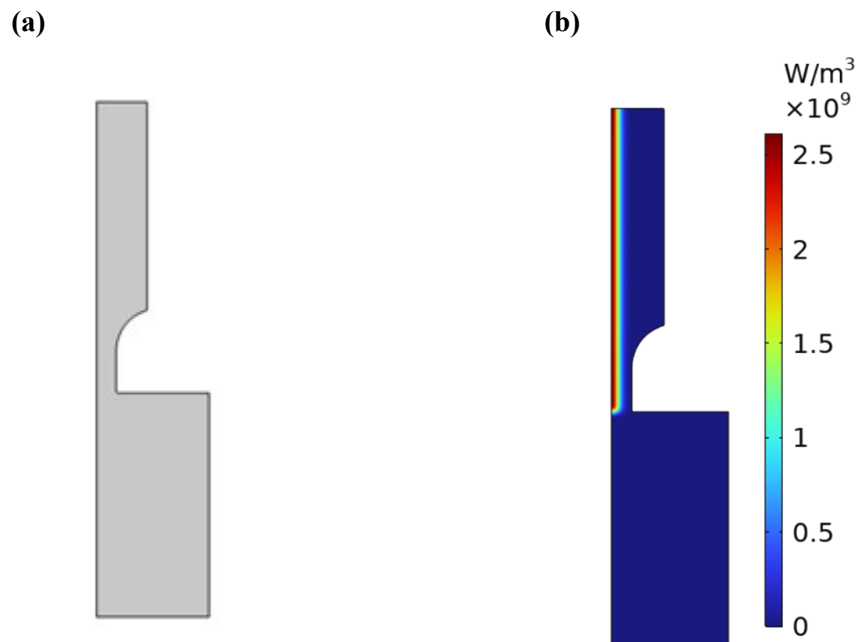


**Figure S5.** (a) 2D axisymmetric geometry of the single GAP model and (b) the heat source ( $\text{W m}^{-3}$ ) to mimic the plasma.

As mentioned in section 3 of the main paper, the model contains a user-defined heat source to mimic the plasma, which is sufficient for the purpose of this study<sup>3, 4</sup>. This heat source is described by a Gaussian pulse in the  $r$  direction, and a rectangular profile in the  $z$  direction, as shown in Figure S5b, and Figure S6. This heat source provides a user-defined power to the model by multiplying the area under the function curves with a constant, resulting in the desired input power (900 W).

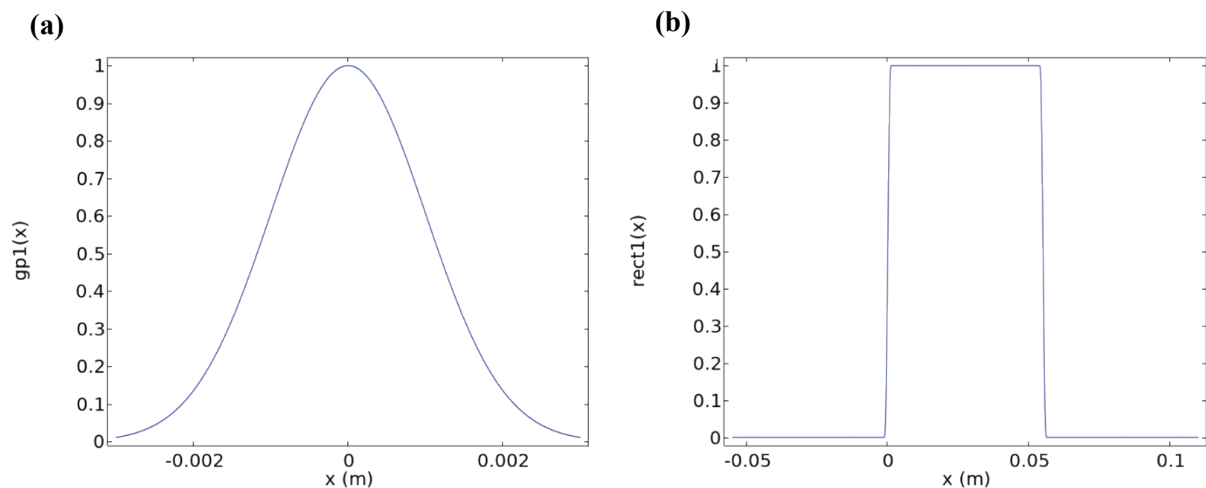


**Figure S6.** Description of the heat source, using (a) a Gaussian function in the r direction and (b) a rectangular function in the z direction.

In this model we use a laminar flow to compute the flow conditions inside the GAP reactor. The flow is calculated by the Navier-Stokes equations (Eqn S1 and S2). In addition to this, the model solves for the heat balance equation through the following heat balance equation<sup>5</sup>:

$$\rho C_p u \cdot \nabla T + \nabla \cdot q = Q \quad (S6)$$

With

$$q = -k \nabla T \quad (S7)$$

Where  $C_p$  ( $\text{J kg}^{-1} \text{K}^{-1}$ ) is the heat capacity of the gas,  $T$  (K) is the gas temperature,  $q$  ( $\text{W m}^{-2}$ ) is the conductive heat flux,  $Q$  ( $\text{W m}^{-3}$ ) is a heat source term, and  $k$  ( $\text{W m}^{-1} \text{K}^{-1}$ ) is the thermal conductivity of the gas.

The boundary conditions for the fluid flow are listed in Table S1. Here,  $\mathbf{u}$  ( $\text{m s}^{-1}$ ) is the velocity vector,  $p_0$  (Pa) is the outlet pressure,  $\mathbf{n}$  is the normal velocity vector to the boundary layer.

**Table S1.** Boundary conditions for the laminar flow equations

|        | $p$ (Pa)              | $u$ ( $\text{m s}^{-1}$ ) |
|--------|-----------------------|---------------------------|
| Inlet  | /                     | $u = u_0$                 |
| Walls  | /                     | $u = 0$                   |
| Outlet | $[-pI + K]n = -p_0 n$ | /                         |

The boundary heat conditions for the heat balance equation are listed in Table S2. Here,  $\Delta H$  ( $\text{J kg}^{-1} \text{K}^{-1}$ ) is the sensible enthalpy.

**Table S2.** Boundary conditions for the heat balance equations

|        | $T$ (K)            | $q$ ( $\text{W m}^{-2}$ )              | $Q$ ( $\text{W m}^{-3}$ ) |
|--------|--------------------|--|---------------------------|
| Inlet  | $T = T_0 = 293.15$ | $-n \cdot q = \rho \Delta H u \cdot n$ | /                         |
| Walls  | /                  | $-n \cdot q = 0$                       | /                         |
| Outlet | /                  | $-n \cdot q = 0$                       | /                         |
| Domain | /                  | /                                      | $Q = Q_0$                 |

The velocity and temperature profile at the outlet of the single GAP reactor model are used as inputs for the post-plasma chamber model (described in detail in the main paper), and are shown in Figure S7. The outlet was taken at  $z = 0.3$  mm on the symmetry axis.

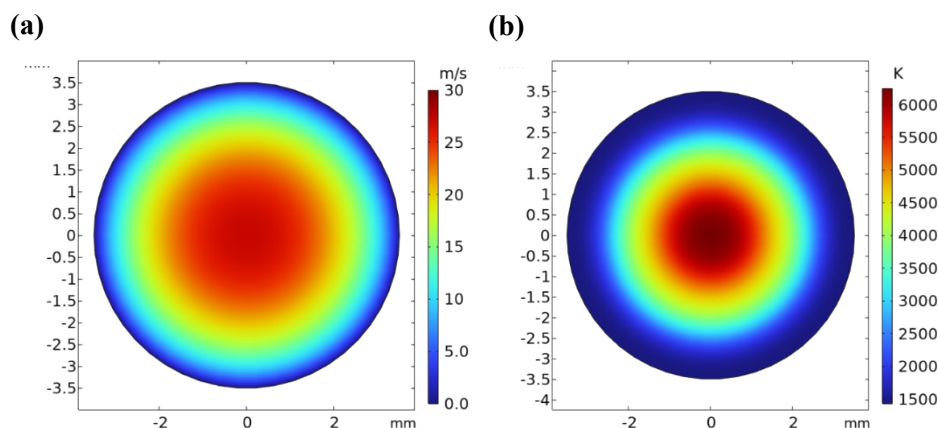


**Figure S7.** (a) Calculated velocity profile ( $\text{m s}^{-1}$ ) and (b) temperature profile of the gas (K) at 0.3 mm (outlet) of the 2D axis-symmetric model.

#### Section S4. Additional information for the 2D post-plasma chamber model

Table S3 lists the number of mesh elements for each simulation of the post-plasma chamber.

**Table S3.** Number of mesh elements for each simulation.

| Simulation | Number of mesh elements |
|------------|-------------------------|
| 35 mm      | 67,859                  |
| 45 mm      | 71,831                  |
| 55 mm      | 77,043                  |
| 65 mm      | 81,820                  |

#### Section S5. Boundary conditions of the 2D post-plasma chamber model

The boundary conditions for the Brinkman equation (Eqn. 12, main text) are listed in Table S4.

**Table S4:** Boundary conditions for the Brinkman equation.

|               | $p$ (Pa)                               | $\mathbf{u}$ ( $\text{m s}^{-1}$ ) |
|---------------|--|------------------------------------|
| Inlet         | /                                      | $\mathbf{u} = \mathbf{u}_0$        |
| Walls         | /                                      | $\mathbf{u} = \mathbf{0}$          |
| Open boundary | $[-pI + K]\mathbf{n} = -f_0\mathbf{n}$ | /                                  |

Here,  $\mathbf{n}$  ( $\text{m s}^{-1}$ ) is the normal vector to the boundary plane and  $\mathbf{u}_0$  ( $\text{m s}^{-1}$ ) is the initial inlet velocity field. The boundary conditions for the heat balance equations (both in the gas and porous medium domains) are listed in Table S5.

**Table S5:** Boundary conditions for the heat balance equations.

|       | $T$ (K)                  | $\mathbf{q}$ ( $\text{W m}^{-2}$ )                                     | $Q$ ( $\text{W m}^{-3}$ ) |
|-------|--------------------------|--|---------------------------|
| Inlet | $T_{ustr} = T_{profile}$ | $-\mathbf{n} \cdot \mathbf{q} = d_z \rho \Delta H u \cdot \mathbf{n},$ | /                         |
|       |                          | $\Delta H = \int_{T_{ustr}}^T C_p dT$                                  |                           |
| Walls | /                        | $-\mathbf{n} \cdot \mathbf{q} = d_z q_0,$                              | /                         |
|       |                          | $q_0 = h(T_{ext} - T),$  |                           |

---

|  |   |                  |           |
|--|---|------------------|-----------|
| $h = 250 \text{ W m}^{-1} \text{ K}^{-1},$ |   |                  |           |
| $T_{ext} = 293.15 \text{ K}$               |   |                  |           |
| Outflow                                    | / | $-n \cdot q = 0$ | /         |
| Domain                                     | / | /                | $Q = Q_0$ |

---

Here,  $T_{ustr}$  (K) is the upstream temperature defined by an imported temperature profile (see SI, Fig. S5b),  $\Delta H$  is the sensible enthalpy,  $q$  ( $\text{W m}^{-2}$ ) is the heat flux,  $q_0$  ( $\text{W m}^{-2}$ ) is the inward heat flux,  $T_{ext}$  (K) is the external temperature and  $Q_0$  ( $\text{W m}^{-3}$ ) is the user-defined heat source (in our case the heat of reaction).

The boundary conditions for the transport of species equation are listed in Table S6.

**Table S6:** Boundary conditions for the transport of concentrated species in porous media.

---

|        | $\omega_i$                                | $J_i$ ( $\text{mol m}^{-2} \text{ s}^{-1}$ ) |
|--------|---|--|
| Inlet  | $\omega_i = \omega_{0,i}$                 | /  |
| Walls  | /   | $-n \cdot j_i = 0$                           |
| Outlet | $-n \cdot \rho D_i^m \nabla \omega_i = 0$ | /  |

---

Here  $\omega_{0,i}$  is the inlet mass fraction,  $j_i$  ( $\text{mol m}^{-2} \text{ s}^{-1}$ ) is the diffusive flux vector of species  $i$  and  $D_i^m$  ( $\text{m}^2 \text{ s}^{-1}$ ) is the mixture-averaged diffusion coefficient.

## Section S6. Temporal change of particle diameter

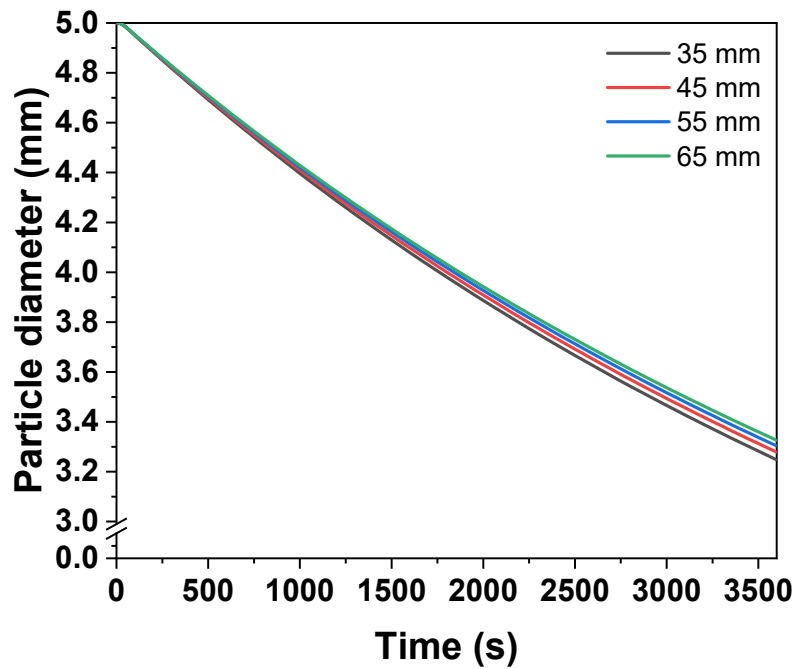


**Figure S8:** Temporal change (s) of the average particle diameter (mm) inside the carbon bed at four distinct locations (35, 45, 55 and 65 mm).

### References

1. G. K. Batchelor, *An introduction to fluid dynamics*, Cambridge university press, 2000.
2. R. Adams, *Calculus Volume 2*, 2022.
3. K. Wang, S. Ceulemans, H. Zhang, I. Tsonev, Y. Zhang, Y. Long, M. Fang, X. Li, J. Yan and A. Bogaerts, *Chemical Engineering Journal*, 2024, **481**, 148684.
4. J.-L. Liu, X. Wang, X.-S. Li, B. Likozar and A.-M. Zhu, *Journal of Physics D: Applied Physics*, 2020, **53**, 253001.
5. *Comsol Multiphysics 6.2 Chemical Reaction Engineering Module User's Guide*.